# Electro-upcycling of PET plastic coupling with hydrogen production using NiCe@NiTe electrocatalyst

Pooja J. Sharma[1], Sanjay A. Bhakhar[1], Manish N. Nandpal[2], Kaushik A. Bhakhar[3], Samir G. Patel[2], Parikshit Sahatiya[4], C.K. Sumesh[1], Pratik M. Pataniya[1,*]

*[1]Department of Physical Sciences, P D Patel Institute of Applied Sciences, Charotar University of Science and Technology, CHARUSAT, Changa, Gujarat, India.*

*[2]Department of Pharmaceutical Chemistry and Analysis, Ramanbhai Patel College of Pharmacy, Charotar University of Science and Technology, CHARUSAT Changa, Gujarat, India.*

*[3]Gandhinagar Institute of Pharmacy, Gandhinagar University, Gandhinagar, Gujarat-382721.*

*[4]Department of Electrical and Electronic Engineering, BITS Pilani Hyderabad, Secunderabad-500078, India.*

**Email:** pm.pataniya9991@gmail.com

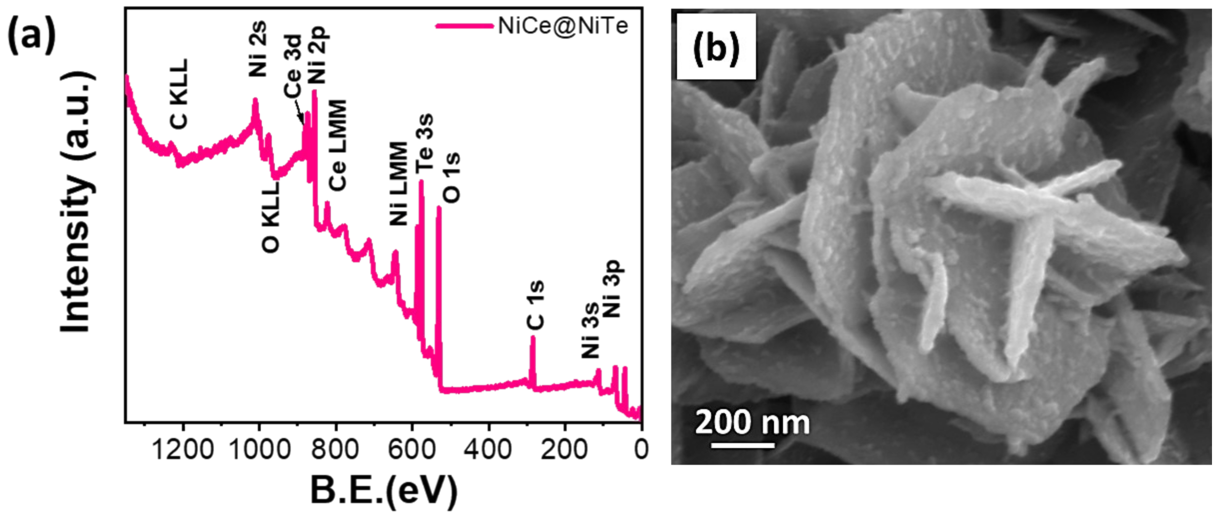


**Figure S1** XPS survey spectra of NiCe@NiTe heterostructure

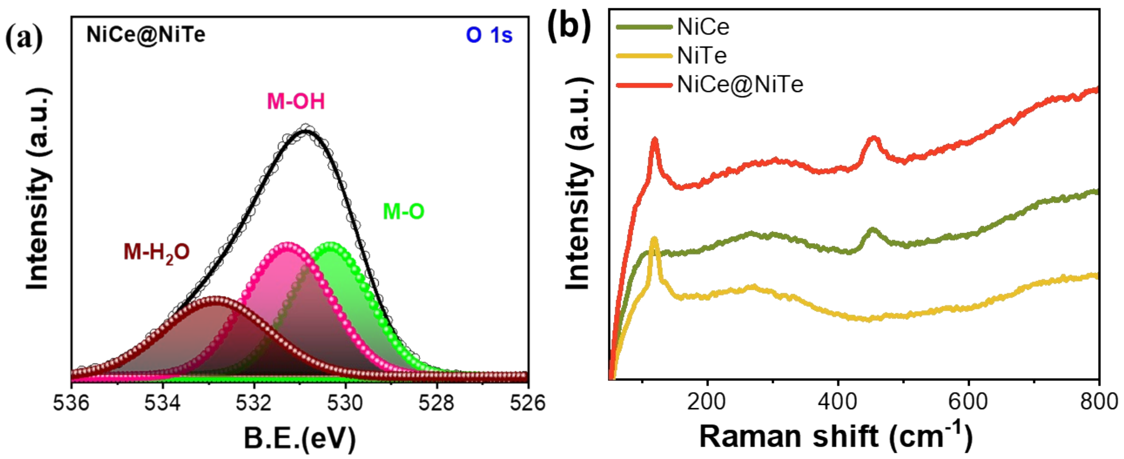


**Figure S2** (a) high-resolution XPS spectra of O 1s, (b) Raman spectra of NiCe, NiTe and NiCe@NiTe electrodes.

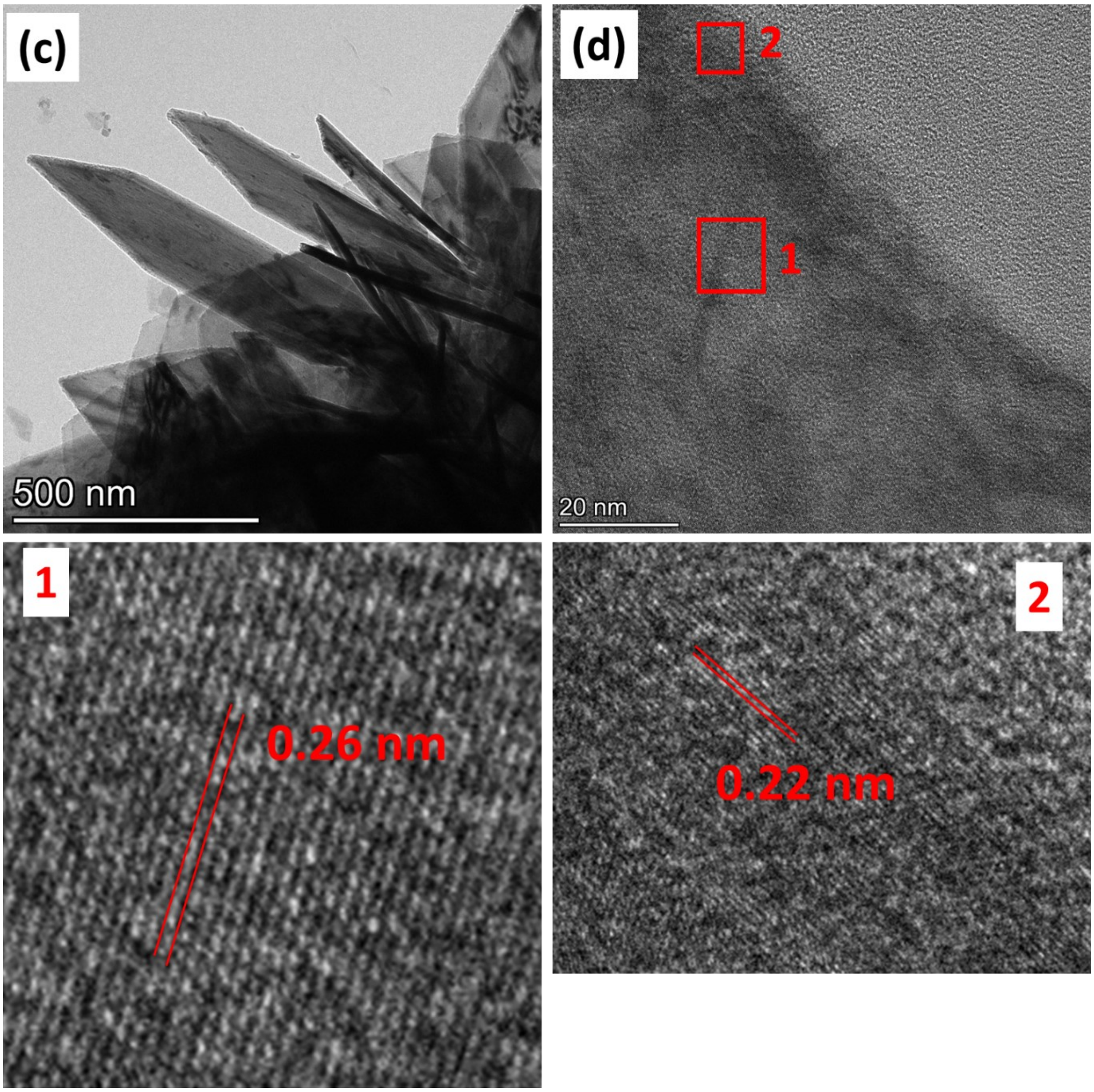


**Figure S2** (c) TEM image of NiCe@NiTe heterostructures, (b) HR-TEM image with region-1 (NiCe LDH) and region-2 (NiTe).

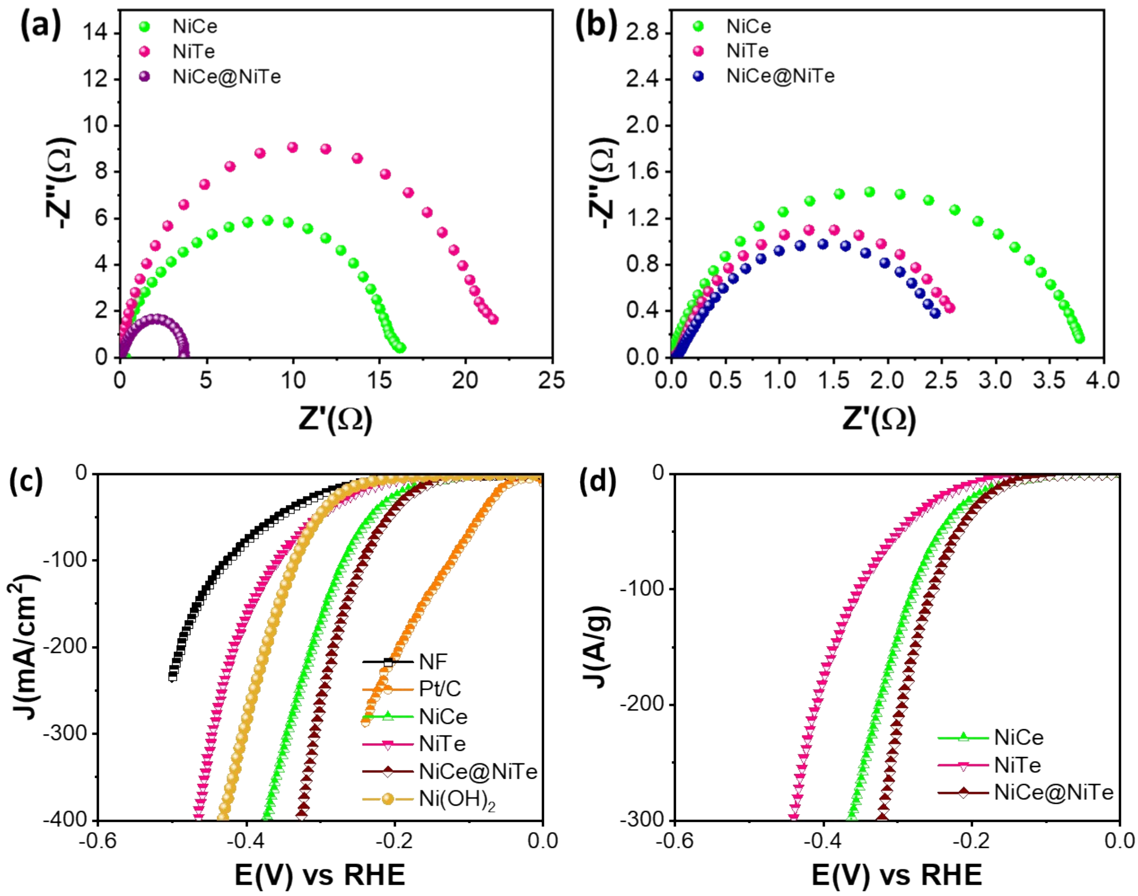


**Figure S3** Nyquist plot of the prepared catalysts in 1.0 M KOH solution (a) HER, (b) OER, (c) Polarization curves for HER, (d) Normalized polarization curve for HER.

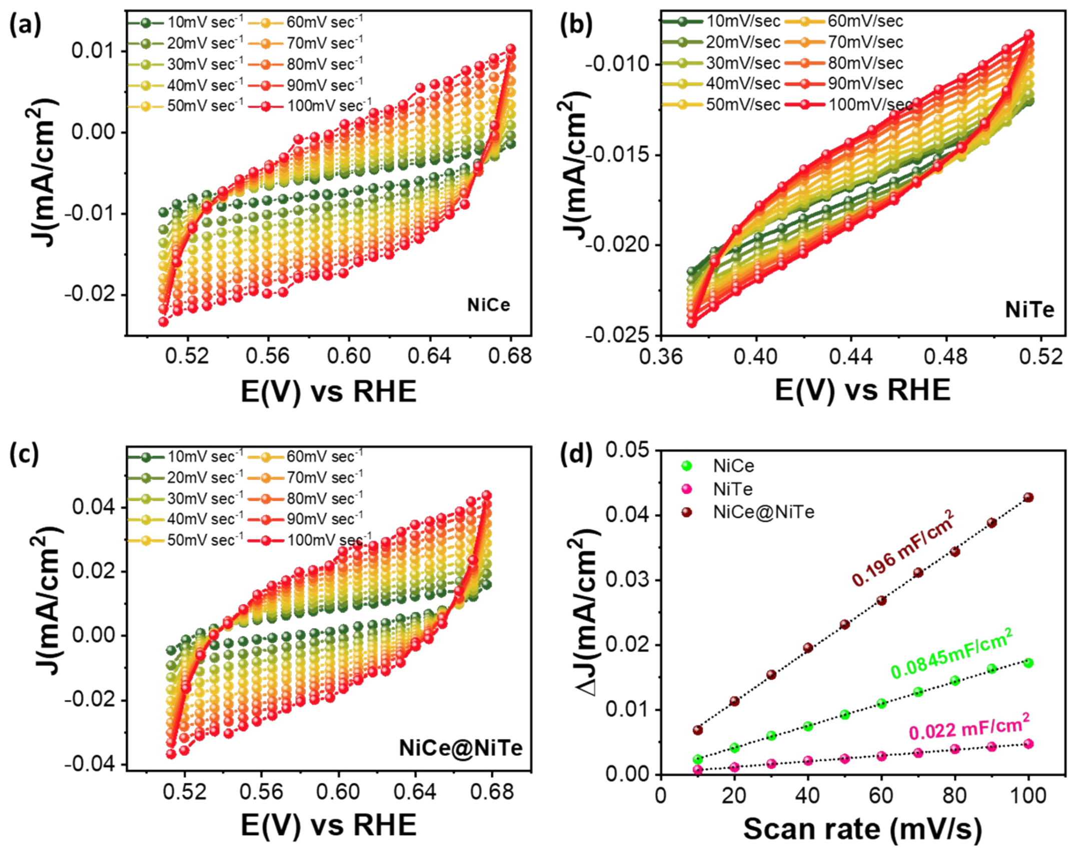


**Figure S4**: (a) CV curve of NiCe, (b) NiTe, and NiCe@NiTe catalysts (d) ΔJ vs scan rate graph.

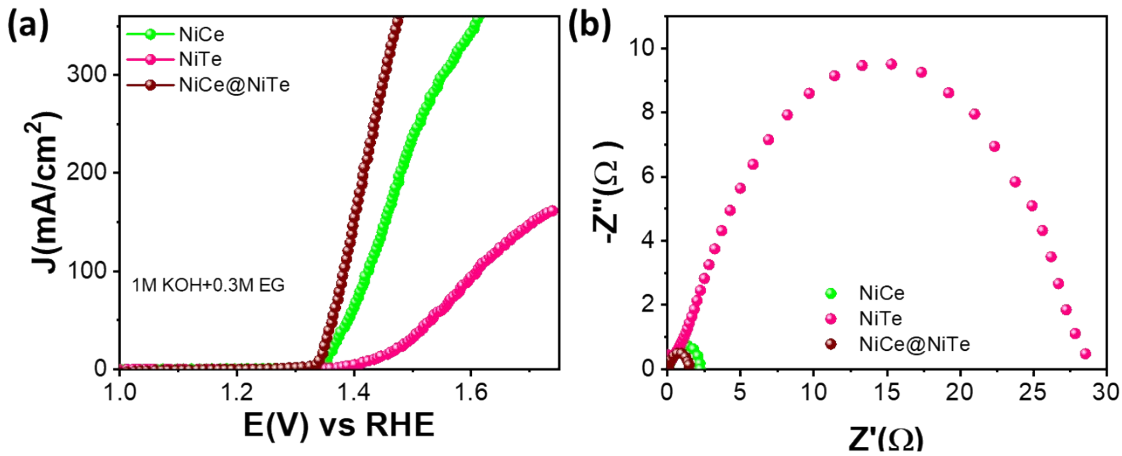

**Figure S5,** (a) LSV polarization curve, and (b) Nyquist plot of the prepared electrodes in 1.0 M KOH +0.3M EG solution.

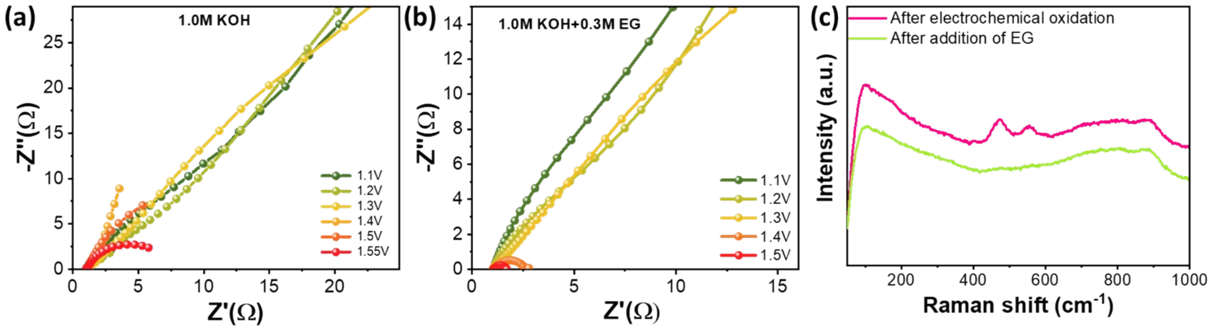


**Figure S6**, Nyquist plot of the prepared catalysts in (a) 1.0 M KOH solution, (b) 1.0M KOH+0.3M EG and (c) in-situ Raman spectroscopy of NiCe@NiTe electrode after electro-oxidation at 1.6 V vs RHE and after addition of EG into electrolyte.

**Quantification of Formate and calculation of the faradic efficiency:**

For the quantification of the formate in the electrolytes was performed using Shimadzu High-Performance Liquid Chromatographic System, Japan (LC-2010 CHT), equipped with PDA detector fitted with quaternary gradient pump, degasser, column oven and autosampler, Luna $C_{18}$ Column (250 mm×4.6 mm; 5μm). After electrolysis at different current densities (10-100 mA/cm$^2$), 1 ml electrolyte was diluted in 9 ml HPLC grade water and used for the recording the chromatograph. The calibration curve was also prepared for the quantification of the formate.

**Optimized Chromatographic Conditions**

| **Parameters** | **Experimental conditions** |
|---|---|
| Instrument | Shimadzu High-Performance Liquid Chromatographic System, Japan (LC-2010 CHT), equipped with PDA detector fitted with quaternary gradient pump, degasser, column oven and autosampler |
| Column | Luna $C_{18}$ Column (250 mm×4.6 mm; 5μm) |
| Mobile phase | 27.5 mM $H_2SO_4$<br>(0.75 mL of $H_2SO_4$ in 500 mL of Milli-Q Water) |
| Mobile phase Ratio | 100 % v/v |
| Flow rate | 0.3 mL/min |
| Diluent | Milli-Q Water |
| Injection volume | 20 μL |
| Column oven temperature | 35 ºC |
| Auto sampler temperature | 15 ºC |

| | |
|---|---|
| Detector | Photo Diode Array (PDA) |
| Lamp | $D_2$ |
| Detection wavelength | 210 nm |
| Software | LabSolutions |
| Run time | 20 minutes |
| These were optimized chromatographic conditions which gives satisfactory results and lie well within acceptance criteria. | |

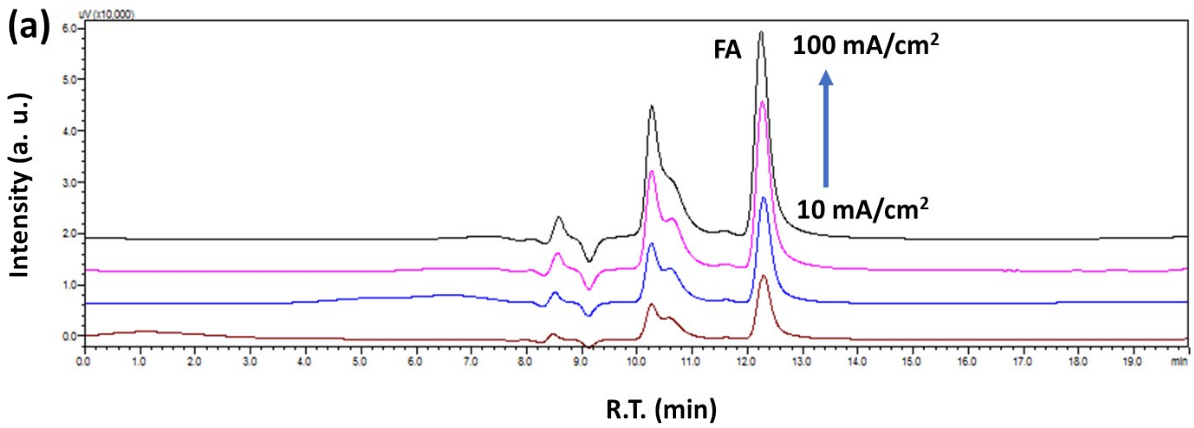


**Figure S7(a)** Stack Chromatogram for conversion from EG to formate (FA) electrolyte at different current for 2 hours.

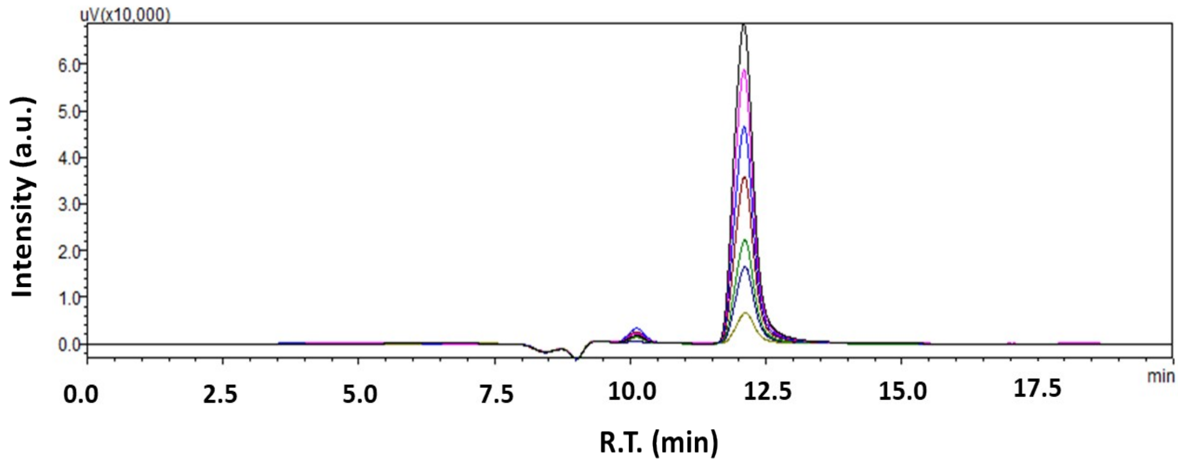


**Figure S7(b)** Stack Chromatogram for formic acid standard for calibration curve for quantification.

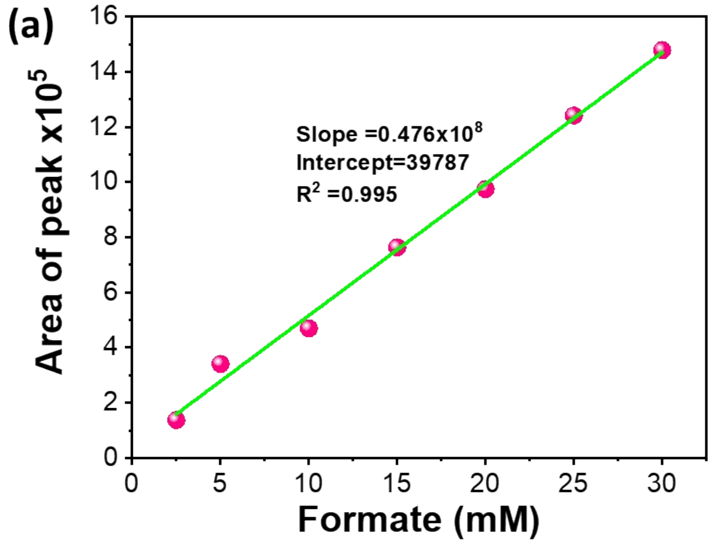


**Figure S7(c)** Calibration curve for quantification of the formate.

Faradic Efficiency for the electrochemical conversion from ethylene glycol to formate was evaluated using following formula:

$$FE(\%) = \frac{2 \times mole\ of\ HCOOH \times 96485}{C} \times 100\%$$

Where, C = charge (C)

**Table S1**. Production rate of formate and faradaic efficieincy at different current densities.

| **Current density ($mA\ cm^{-2}$)** | **Charge (C)** | **Formate Production ($m\ mol\ h^{-1}\ cm^{-2}$)** | **FE (%)** |
|---|---|---|---|
| **10** | 36 | 0.18 | 96.5 |
| **20** | 72 | 0.32 | 85.8 |
| **50** | 180 | 0.55 | 59.0 |
| **100** | 360 | 0.69 | 37.0 |

**Figure S8**, PET plastic bottle

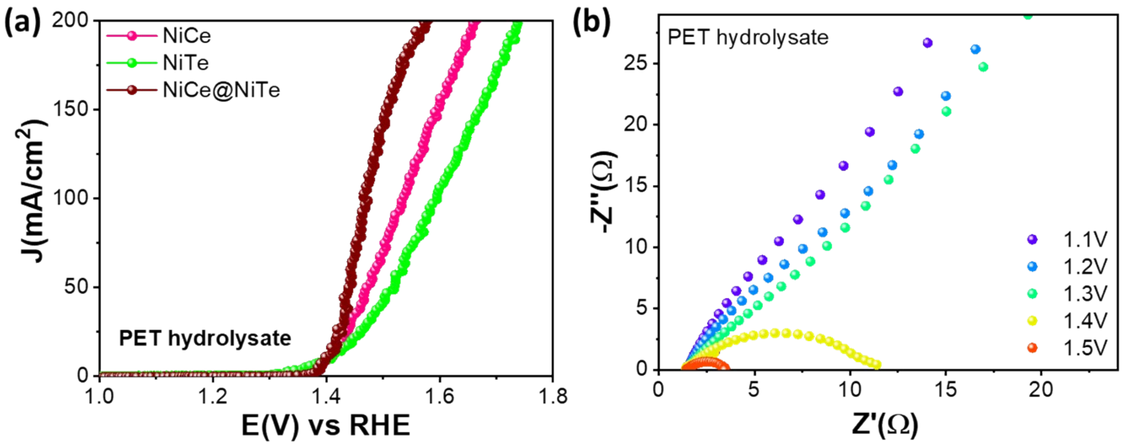


**Figure S9,** (a) LSV polarization curve of the prepared electrodes and (b)Nyquist plot of NiCe@NiTe catalyst in PET hydrolysate.

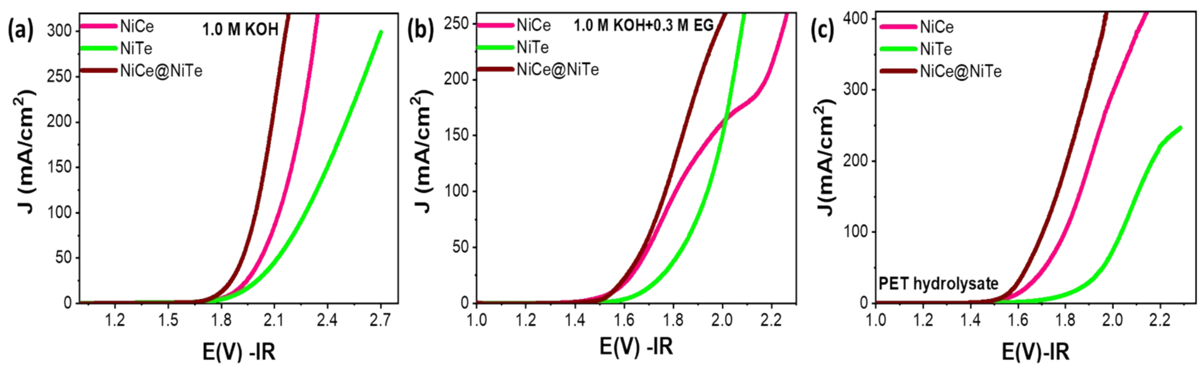


**Figure S10** LSV curve of the prepared electrocatalysts in (a) 1.0M KOH, (b) 1.0M KOH+0.3M EG, and (c) PET hydrolysate solution.

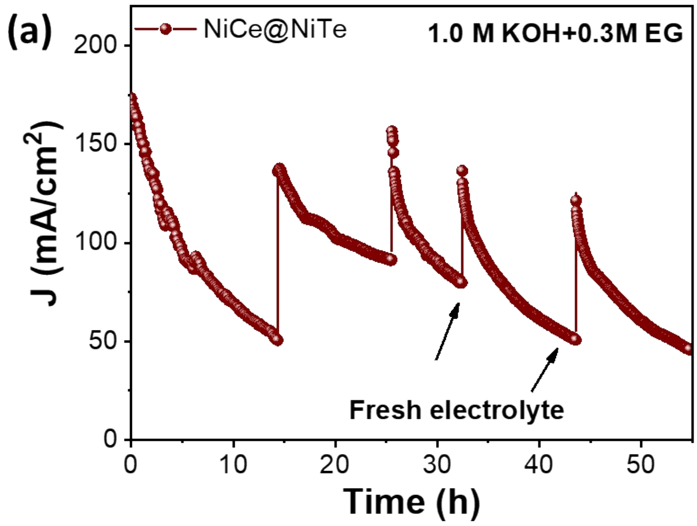


**Figure S11** Stability of NiCe@NiTe catalysts in 1.0M KOH+0.3M EG solution.

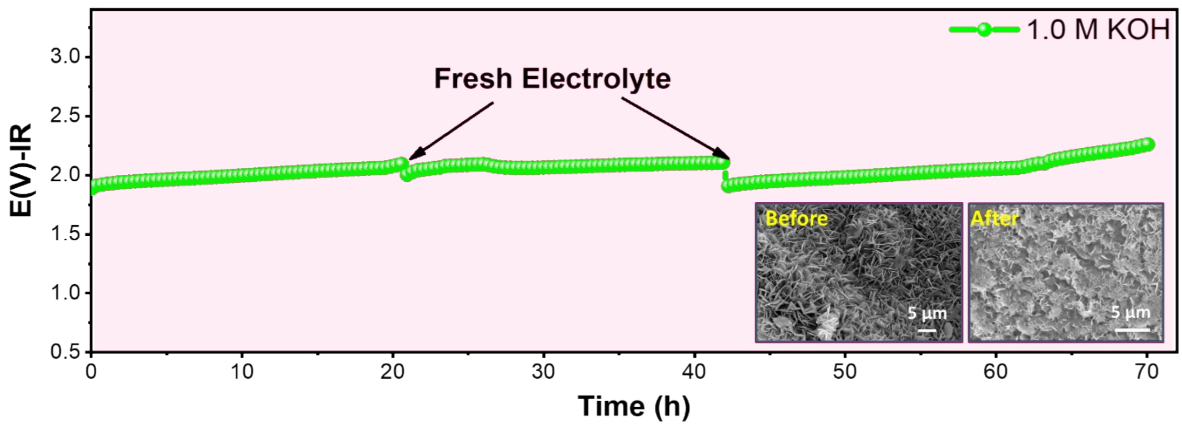


**Figure S12** Stability of NiCe@NiTe catalysts in 1M KOH.

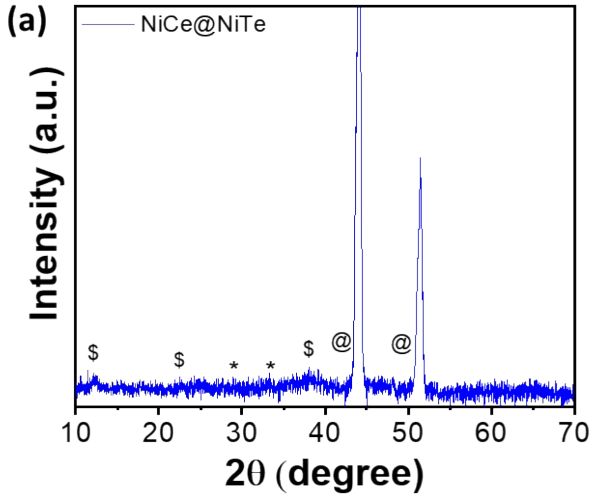


**Figure S13** XRD pattern of NiCe@NiTe catalysts after 100 h stability in 1.0M KOH solution.

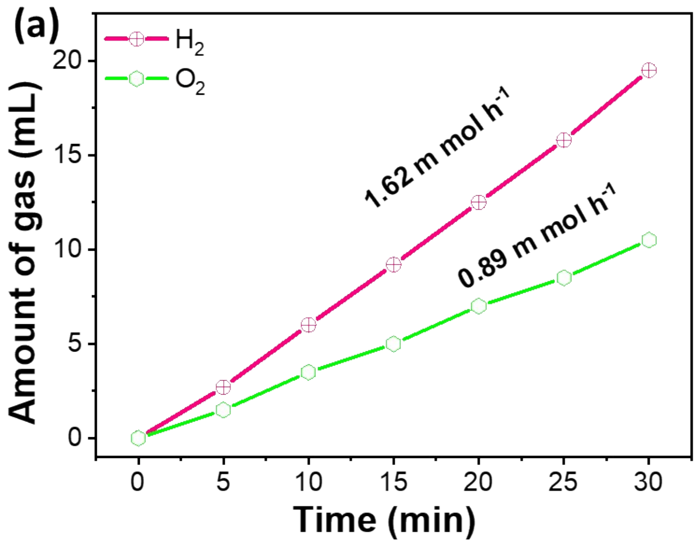


**Figure S14** varying amount of $H_2$ and $O_2$ gas with time

**Table S2** Comparison of the performance of different advanced HER electrocatalysts.

| No. | Catalyst | Electrolyte | Potential (V vs.RHE) for 100 mA cm$^{-2}$ | Ref. |
|---|---|---|---|---|
| 1. | NiCe@NiTe | 1M KOH | 150mV @10 mA/cm$^2$<br>243mV@100 mA/cm$^2$ | **This work** |
| 2. | $NiSe_2$//$Ni(OH)_2$ | 1M KOH | 184mV@10 mA/cm$^2$ | [1] |
| 3. | NiCoFeB nanochains | 1M KOH | 345mV@10 mA/cm$^2$ | [2] |
| 4. | PO-Ni/Ni–N-CNFs | 1M KOH | 262mV@10 mA/cm$^2$ | [3] |
| 5. | $CoS_2$/$MoS_2$/NF | 1M KOH | 180mV@10 mA/cm$^2$<br>358mV@100 mA/cm$^2$ | [4] |
| 6. | $Ni_3S_2$\|P | 1M KOH | 298mV@100 mA/cm$^2$ | [5] |
| 7. | ($NiCo_2S_4$ NS/CC) | 1M KOH | 181mV@10 mA/cm$^2$ | [6] |

| | | | | |
|---|---|---|---|---|
| 8. | $Fe_2V$-MOF | 1M KOH | 198mV@10 mA/cm$^2$ | [7] |
| 9. | $CoFeN_x$HNAs/NF | 1M KOH | 200mV@10 mA/cm$^2$ | [8] |
| 10. | ($NiCo_2S_4$ NS/CC) | 1M KOH | 181mV@10 mA/cm$^2$ ~330mV@100 mA/cm$^2$ | [6] |
| 11. | B, N: $Mo_2C$@BCN | 1M KOH | 148mV@10 mA/cm$^2$ 273mV@100mA/cm$^2$ | [9] |
| 12. | NiFeP nanorods | 1M KOH | 178mV@10 mA/cm$^2$ | [10] |
| 13. | NiCoFeP/C | 1M KOH | 149mV@10 mA/cm$^2$ | [11] |
| 14. | $Co_2P/Mo_2C/Mo_3Co3C$@C | 1M KOH | 182mV@10 mA/cm$^2$ | [12] |
| | | | | |

**Table S3** Comparison of the performance of different advanced OER electrocatalysts.

| No. | Catalyst | Electrolyte | Potential (V vs.RHE) | Ref. |
|---|---|---|---|---|
| 1. | NiCe@NiTe | 1M KOH | 1.54V@10 mA/cm$^2$ 1.63V@100 mA/cm$^2$ | **This work** |
| 2. | ZIF-12/Fe-Cu | 1M KOH | 1.567@10 mA/cm$^2$ | [13] |
| 3. | NiFeSe@NiSe/O@CC | 1M KOH | 1.56V @10mA/cm$^2$ | [14] |
| 2. | $Ni_3S_2$\|P | 1M KOH | 1.65V@100 mA/cm$^2$ | [15] |
| 3. | $NiSe_2$//$Ni(OH)_2$ | 1M KOH | 1.645V@10 mA/cm$^2$ | [1] |
| 4. | $Ni_{0.6}Fe_{0.4}$/C | 1M KOH | 1.57V@10mA/m$^2$ | [16] |
| 5. | $NiS_2/CoS_2$ | 1M KOH | 1.635V@100 mA/cm$^2$ | [17] |
| 6. | Ni/VN/NF | 1M KOH | 1.56V@10 mA/cm$^2$ 1.63V@100 mA/cm$^2$ | [18] |
| 7. | NiFe LDH | 1M KOH | 1.58V @10mA/cm$^2$ | [19] |
| 8. | Ni MOF (BTC) | 1M KOH | 1.576V @10 mA/cm$^2$ | [20] |
| 9. | 2D Ni-BDC/$Ni(OH)_2$ | 1M KOH | 1.55V@10 mA/cm$^2$ | [21] |
| 10. | Co-Fe-P-Se/NC | 1M KOH | 1.50V@10 mA/cm$^2$ | [22] |
| 11. | NiCoFeP/C | 1M KOH | 1.50V@10 mA/cm$^2$ | [11] |
| 12. | $Co_2P/Mo_2C/Mo_3Co3C$@C | 1M KOH | 1.592V@10 mA/cm$^2$ | [12] |

**Table S4** Comparison of PETOR and EGOR performance of NiCe@NiTe catalysts with previous reports work.

| Catalyst | Electrolyte | Potential (V vs.RHE) for 100 mA cm$^{-2}$ | Ref. |
|---|---|---|---|
| NiCe@NiTe | PET Hydrolysate | 1.4V @10mA/cm$^2$ 1.46V @100mA/cm$^2$ | **This work** |
| $Mn_{0.1}Ni_{0.9}Co_2O_{4-\delta}$ RSFs/CFP | PET Hydrolysate | 1.43V @50mA/cm2 | [23] |
| OMS-$Ni_1$-CoP | PET Hydrolysate | 1.52 V @ 10 mA/cm$^2$ | [24] |
| $Ni_3N/W_5N_4$ | PET Hydrolysate | 1.47 V @ 50 mA/cm$^2$ | [25] |
| $CuCo_2O_4$/NF | PET Hydrolysate | 1.56 V @ 100 mA/cm$^2$ | [26] |
| Co, Cl-NiS | PET electrooxidation | 1.51V @100mA/cm$^2$ | [27] |

| | | | |
|---|---|---|---|
| NiCe@NiTe | 1.0M KOH+0.3M EG | 1.34V @10 mA/cm$^2$<br>1.38V@100 mA/cm$^2$ | **This work** |
| $NiCo_2O_4$/CFP | 1 M NaOH + 0.1 M EG | 1.44V @50mA/cm2 | [28] |
| OMS-Ni1- CoP | 1 M KOH + 0.5 M EG | 1.38V @50mA/cm$^2$ | [24] |
| Cobalt-Based Coordination Polymer | 1 M KOH + 0.1 M EG | 1.42V @10mA/cm$^2$ | [29] |
| Ni-$Fe_3Se_4$ | 1M KOH + 0.3 M EG | 1.49 @ 10 mA/cm$^2$ | [30] |

**Table S5** Comparison of overall water splitting performance of NiCe@NiTe with previous reports work.

| Catalysts | Potential (V)@current density (mA/cm$^2$) | Ref. |
|---|---|---|
| NiCe@NiTe | 1.78V @10 mA/cm$^2$<br>1.99V@100mA/cm$^2$ | **This work** |
| CoMoO//CoMoP NSs@NF | ~ 1.9V@100 mA/cm$^2$ | [5] |
| CoNi/$CoFe_2O_4$/NF | 1.75V @ 100 mA cm$^{-2}$ | [31] |
| $Co_{0.26}$-$Ni(OH)_2$/CF | 1.73V@10 mA/cm$^2$<br>1.9V@100 mA/cm$^2$ | [32] |
| NiCoFeB nanochains | 1.81V@10 mA/cm$^2$<br>1.96V@100 mA/cm$^2$ | [2] |
| B, N: $Mo_2C$@BCN | 1.84V@100 mA/cm$^2$ | [9] |
| CoMn/$CoMn_2O_4$ | 1.64V@10 mA/cm$^2$<br>1.91V@100 mA/cm$^2$ | [33] |
| NiCoFeP/C | 1.6V@10 mA/cm$^2$ | [11] |
| $Co_2P/Mo_2C/Mo_3Co3C$@C | 1.74V@10 mA/cm$^2$ | [12] |
| NiMoP-NiFeP | 1.57V@10 mA/cm$^2$ | [34] |

**References:**

[1] H. Liang, L. Li, F. Meng, L. Dang, J. Zhuo, A. Forticaux, Z. Wang, S. Jin, Porous two-dimensional nanosheets converted from layered double hydroxides and their applications in electrocatalytic water splitting, Chem. Mater. 27 (2015) 5702–5711.

[2] Y. Li, B. Huang, Y. Sun, M. Luo, Y. Yang, Y. Qin, L. Wang, C. Li, F. Lv, W. Zhang, Multimetal borides nanochains as efficient electrocatalysts for overall water splitting,

Small. 15 (2019) 1804212.

[3] Z.-Y. Wu, W.-B. Ji, B.-C. Hu, H.-W. Liang, X.-X. Xu, Z.-L. Yu, B.-Y. Li, S.-H. Yu, Partially oxidized Ni nanoparticles supported on Ni-N co-doped carbon nanofibers as bifunctional electrocatalysts for overall water splitting, Nano Energy. 51 (2018) 286–293.

[4] J. Zhu, X. Zheng, Y. Lu, H. Tong, M. Qi, Y. Liu, D. Li, D. Jiang, Synergistic Coupling of CoS2/MoS2 with Polypyrrole as a Highly Efficient and Robust Bifunctional Electrocatalyst for Water Splitting, ACS Sustain. Chem. Eng. 12 (2023) 235–247.

[5] Y. Zhang, Q. Shao, S. Long, X. Huang, Cobalt-molybdenum nanosheet arrays as highly efficient and stable earth-abundant electrocatalysts for overall water splitting, Nano Energy. 45 (2018) 448–455.

[6] W. Zhu, M. Ren, N. Hu, W. Zhang, Z. Luo, R. Wang, J. Wang, L. Huang, Y. Suo, J. Wang, Traditional NiCo2S4 phase with porous nanosheets array topology on carbon cloth: a flexible, versatile and fabulous electrocatalyst for overall water and urea electrolysis, ACS Sustain. Chem. Eng. 6 (2018) 5011–5020.

[7] Y. Kong, D. Xiong, C. Lu, J. Wang, T. Liu, S. Ying, X. Ma, F.Y. Yi, Vanadium-Based Trimetallic Metal-Organic-Framework Family as Extremely High-Performing and Ultrastable Electrocatalysts for Water Splitting, ACS Appl. Mater. Interfaces. 14 (2022) 37804–37813. https://doi.org/10.1021/acsami.2c09998.

[8] D. Li, Y. Xing, R. Yang, T. Wen, D. Jiang, W. Shi, S. Yuan, Holey cobalt–iron nitride nanosheet arrays as high-performance bifunctional electrocatalysts for overall water splitting, ACS Appl. Mater. Interfaces. 12 (2020) 29253–29263.

[9] M.A.R. Anjum, M.H. Lee, J.S. Lee, Boron-and nitrogen-codoped molybdenum carbide nanoparticles imbedded in a BCN network as a bifunctional electrocatalyst for hydrogen and oxygen evolution reactions, ACS Catal. 8 (2018) 8296–8305.

[10] Y. Du, Z. Li, Y. Liu, Y. Yang, L. Wang, Nickel-iron phosphides nanorods derived from bimetallic-organic frameworks for hydrogen evolution reaction, Appl. Surf. Sci. 457 (2018) 1081–1086.

[11] X. Wei, Y. Zhang, H. He, L. Peng, S. Xiao, S. Yao, P. Xiao, Carbon-incorporated porous honeycomb NiCoFe phosphide nanospheres derived from a MOF precursor for overall water splitting, Chem. Commun. 55 (2019) 10896–10899.

[12] X. Li, X. Wang, J. Zhou, L. Han, C. Sun, Q. Wang, Z. Su, Ternary hybrids as efficient bifunctional electrocatalysts derived from bimetallic metal–organic-frameworks for overall water splitting, J. Mater. Chem. A. 6 (2018) 5789–5796.

[13] S. Shi, B. Wang, Y. Wang, Y. Yang, Z. Zhang, Y. Xu, Y. Suo, Structure optimization of ZIF-12-derived Co-NC for efficient oxygen reduction and oxygen evolution, Fuel. 330 (2022) 125516.

[14] G. Yilmaz, C.F. Tan, Y.-F. Lim, G.W. Ho, Pseudomorphic Transformation of Interpenetrated Prussian Blue Analogs into Defective Nickel Iron Selenides for Enhanced Electrochemical and Photo-Electrochemical Water Splitting, Adv. Energy Mater. 9 (2019) 1802983. https://doi.org/https://doi.org/10.1002/aenm.201802983.

[15] Q. Liu, L. Wei, Q. Liu, G. Chen, X. Kong, Anion Engineering on 3D Ni3S2 Nanosheets Array toward Water Splitting, ACS Appl. Energy Mater. 1 (2018) 3488–

3496. https://doi.org/10.1021/acsaem.8b00710.

[16] Y. Liu, Y. Wang, Y. Zhao, L. Liu, S. Liu, D. Zhang, H. Wu, B. Jia, L. Zhang, M. Qin, High-frequency ultrasonic pyrolysis of 200 nm ultrafine Fe-doped NiO hollow spheres for efficient oxygen evolution catalysis, New J. Chem. 46 (2022) 19685–19693.

[17] J. Yin, Y. Li, F. Lv, M. Lu, K. Sun, W. Wang, L. Wang, F. Cheng, Y. Li, P. Xi, S. Guo, Oxygen Vacancies Dominated NiS2/CoS2 Interface Porous Nanowires for Portable Zn–Air Batteries Driven Water Splitting Devices, Adv. Mater. 29 (2017) 1–8. https://doi.org/10.1002/adma.201704681.

[18] Q. Li, P. Yang, Y. Liu, W. Xiao, Z. Xiao, G. Xu, L. Wang, F. Liu, Z. Wu, In-situ construction of pomegranate-like nickel-vanadium nitride for hydrogen production through urea-assisted water-splitting, J. Alloys Compd. 968 (2023) 171861.

[19] F. Song, X. Hu, Exfoliation of layered double hydroxides for enhanced oxygen evolution catalysis, Nat. Commun. 5 (2014) 4477.

[20] V. Maruthapandian, S. Kumaraguru, S. Mohan, V. Saraswathy, S. Muralidharan, An insight on the electrocatalytic mechanistic study of pristine Ni MOF (BTC) in alkaline medium for enhanced OER and UOR, ChemElectroChem. 5 (2018) 2795–2807.

[21] D. Zhu, J. Liu, L. Wang, Y. Du, Y. Zheng, K. Davey, S.-Z. Qiao, A 2D metal–organic framework/Ni (OH) 2 heterostructure for an enhanced oxygen evolution reaction, Nanoscale. 11 (2019) 3599–3605.

[22] H. Wu, J. Wang, J. Yan, Z. Wu, W. Jin, MOF-derived two-dimensional N-doped carbon nanosheets coupled with Co–Fe–P–Se as efficient bifunctional OER/ORR catalysts, Nanoscale. 11 (2019) 20144–20150.

[23] Y. Mao, S. Fan, X. Li, J. Shi, M. Wang, Z. Niu, G. Chen, Trash to treasure: electrocatalytic upcycling of polyethylene terephthalate (PET) microplastic to value-added products by Mn0. 1Ni0. 9Co2O4-δ RSFs spinel, J. Hazard. Mater. 457 (2023) 131743.

[24] N. Wang, X. Li, M.-K. Hu, W. Wei, S.-H. Zhou, X.-T. Wu, Q.-L. Zhu, Ordered macroporous superstructure of bifunctional cobalt phosphide with heteroatomic modification for paired hydrogen production and polyethylene terephthalate plastic recycling, Appl. Catal. B Environ. 316 (2022) 121667. https://doi.org/https://doi.org/10.1016/j.apcatb.2022.121667.

[25] F. Ma, S. Wang, X. Gong, X. Liu, Z. Wang, P. Wang, Y. Liu, H. Cheng, Y. Dai, Z. Zheng, B. Huang, Highly efficient electrocatalytic hydrogen evolution coupled with upcycling of microplastics in seawater enabled via Ni3N/W5N4 janus nanostructures, Appl. Catal. B Environ. Energy. 307 (2022) 121198. https://doi.org/https://doi.org/10.1016/j.apcatb.2022.121198.

[26] F. Liu, X. Gao, R. Shi, E.C.M. Tse, Y. Chen, A general electrochemical strategy for upcycling polyester plastics into added-value chemicals by a CuCo2O4 catalyst, Green Chem. 24 (2022) 6571–6577. https://doi.org/10.1039/D2GC02049A.

[27] Z. Chen, R. Zheng, T. Bao, T. Ma, W. Wei, Y. Shen, B.-J. Ni, Dual-Doped Nickel Sulfide for Electro-Upgrading Polyethylene Terephthalate into Valuable Chemicals and Hydrogen Fuel, Nano-Micro Lett. 15 (2023) 210. https://doi.org/10.1007/s40820-023-01181-8.

[28] J. Wang, X. Li, M. Wang, T. Zhang, X. Chai, J. Lu, T. Wang, Y. Zhao, D. Ma, Electrocatalytic Valorization of Poly(ethylene terephthalate) Plastic and CO2 for Simultaneous Production of Formic Acid, ACS Catal. 12 (2022) 6722–6728. https://doi.org/10.1021/acscatal.2c01128.

[29] S. Behera, S. Dinda, R. Saha, B. Mondal, Quantitative electrocatalytic upcycling of polyethylene terephthalate plastic and its oligomer with a cobalt-based one-dimensional coordination polymer having open metal sites along with coproduction of hydrogen, ACS Catal. 13 (2022) 469–474.

[30] P.M. Pataniya, P.J. Sharma, S.A. Bhakhar, M. Patel, M. Nandpal, K.A. Bhakhar, S. Patel, P. Sahatiya, G. Nagaraju, C.K. Sumesh, Binder-free Nickel Iron Selenide Catalyst arrays for coupling hydrogen production with polyethylene terephthalate plastic electro-upcycling, J. Mater. Chem. A. (2025). https://doi.org/10.1039/D5TA06515A.

[31] S. Li, S. Sirisomboonchai, A. Yoshida, X. An, X. Hao, A. Abudula, G. Guan, Bifunctional CoNi/CoFe 2 O 4/Ni foam electrodes for efficient overall water splitting at a high current density, J. Mater. Chem. A. 6 (2018) 19221–19230.

[32] C.B. Sun, M.W. Guo, S.S. Siwal, Q.B. Zhang, Efficient hydrogen production via urea electrolysis with cobalt doped nickel hydroxide-riched hybrid films: Cobalt doping effect and mechanism aspect, J. Catal. 381 (2020) 454–461. https://doi.org/https://doi.org/10.1016/j.jcat.2019.11.034.

[33] D. Zheng, Z. Jing, Q. Zhao, Y. Kim, P. Li, H. Xu, Z. Li, J. Lin, Efficient Co-doped pyrrhotite Fe0. 95S1. 05 nanoplates for electrochemical water splitting, Chem. Eng. J. 402 (2020) 125069.

[34] H. Roh, H. Jung, H. Choi, J.W. Han, T. Park, S. Kim, K. Yong, Various metal (Fe, Mo, V, Co)-doped Ni2P nanowire arrays as overall water splitting electrocatalysts and their applications in unassisted solar hydrogen production with STH 14%, Appl. Catal. B Environ. 297 (2021) 120434.